ChemSusChem

Full Papers
doi.org/10.1002/cssc.202100893

Chemistry Europe
European Chemical
Societies Publishing

r...t...l c ro ic Co li o C₃W -W₂C ʼ cor... R Cl r a R r bl C... o ... l croc...t ic ...ro... ...o... ...q...o R...t io

Yuting Yang,[a] Xue Shao,[a] Shuqing Zhou,[a] Puxuan Yan,[a] Tayirjan Taylor Isimjan,*[b] and Xiulin Yang*[a]

Designing a bifunctional catalyst for hydrogen oxidation reaction (HOR) and hydrogen evolution reaction (HER) is significant toward developing sustainable hydrogen-electric conversion systems. Herein, a cost-effective bifunctional catalyst, Ru/N-doped Carbon@WO$_3$-W$_2$C (Ru/NC@WOC), was developed via co-precipitation and polyol reduction. Ru/NC@WOC showed superior HOR/HER activity in alkaline solution in comparison with commercial Pt/C. HOR electrochemical tests showed that the mass activity at 0.05 V (1.96 mAμg_{Ru}^{-1}) and exchange-current density were 7.5 and 1.2 times that of Pt/C. Additionality, Ru/NC@WOC exhibited up 30-fold HOR activity in mass activity compared with benchmark Ru/C. Moreover, it also displayed exceptional electrocatalytic HER with overpotentials of 31 mV at 10 mA cm^{-2} and 119 mV at 100 mA cm^{-2}, surpassing Pt/C, benchmark Ru/C, and most of the previously reported electrocatalysts. The outstanding catalytic activity of Ru/NC@WOC probably arises from the synergy between Ru and NC@WOC matrix, suitable hydrogen binding energy, and highly conductive substrate. Thus, this work may pave a new avenue to fabricate low-cost bifunctional HOR/HER catalysts for alkaline fuel cells and water electrolyzer.

ro...c io

With the severe energy shortage and negative environmental issues due to the rapid depletion of traditional fossil fuels, it is exigent to develop green, renewable, and highly efficient energy sources.[1] Hydrogen generated through water electrolysis is a practical approach to reduce our excessive reliance on conventional fossil fuels.[2] For the reversible hydrogen electrode (RHE) reactions, involving hydrogen oxidation reaction (HOR) and hydrogen evolution reaction (HER), HOR predominantly finds application on the anode of fuel cells and HER features in water electrolysis.[3] Proton exchange membrane fuel cells (PEMFCs) have gained substantial attentions owing to high power efficiency and high energy density.[1d] However, PEMFCs operate in a strong acidic condition and rely on expensive Pt-based catalysts.[4] As a result; alkaline anion-exchange membrane fuel cells (AAEMFCs) and water electrolyzers have been regarded as a promising alternatives to the PEMFC-based devices.[5] Subsequently, the rapid development of AAEMFCs has motivated searches for active HOR/HER electrocatalysts in alkaline conditions. In particular, designing reversible catalysts for HOR/HER appears to be critical since it can work in the reversible fuel cell, including hydrogen oxidation in the fuel-cell mode and hydrogen evolution in the water-electrolysis mode to realize the reversible production and utilization of hydrogen.[6] To date, Pt and Pt-based catalysts are the optimal HOR/HER electrocatalysts. However, the alkaline HOR/HER activity of Pt is sluggish, approximately two to three orders of magnitude less active than in acid, which means a very high Pt loading is required in alkaline media.[7] Thus, developing highly efficient, cost-effective, and stable HOR/HER catalysts is of immense economic significance. In order to design new efficient HOR/HER electrocatalysts, fundamentally understanding the HOR/HER reaction mechanisms in an alkaline medium is necessary.

A bifunctional mechanism was reported in a previous work to explain the performance of HOR/HER under alkaline media:[8] (1) adsorbed OH (oxophilicity) on the metal, (2) strength of hydrogen binding energy (HBE) on metal, and (3) maximized electrocatalyst–oxide interface. Markovic and co-workers have shown adding oxophilic components (e.g., Ru) can enhance the HOR/HER activity compared with monometallic Pt.[8c] Qiu et al. verified that much stronger adsorbed OH on the PdCu's *bcc* phase reveals the higher HOR mass and specific activities than that of the *fcc* phase.[9] Nevertheless, the OH$_{ads}$ desorption from oxophilic components is more challenging than the H$_{ads}$ desorption through the catalyst's surface, resulting in higher energy barriers of H$_2$O$_{ads}$ desorption.[10] Durst et al. designed new and advanced electrocatalysts with tuned H-binding energies for HOR/HER, pointing to the importance of HBE toward the activity for HOR/HER.[11] Yan and co-workers have also demonstrated that alkaline HOR/HER activities can be

[a] Y. Yang, X. Shao, S. Zhou, P. Yan, Prof. Dr. X. Yang
Guangxi Key Laboratory of Low Carbon Energy Materials
School of Chemistry and Pharmaceutical Sciences
Guangxi Normal University
Guilin 541004 (P. R. China)
E-mail: xlyang@gxnu.edu.cn
[b] Dr. T. T. Isimjan
Saudi Arabia Basic Industries Corporation (SABIC) at King Abdullah University of Science and Technology (KAUST)
Thuwal 23955-6900 (Saudi Arabia)
E-mail: isimjant@sabic.com

Supporting information for this article is available on the WWW under https://doi.org/10.1002/cssc.202100893

related to the HBE as volcano-shaped curves illustrate the HBE plays a crucial role toward HOR/HER.[12] Samanta et al. showed that HBE and oxophilic property may play equally important roles for HOR/HER in the alkaline medium.[4] Meanwhile, Speck et al. demonstrated that maximizing the metal and metal oxide interface is crucial to HOR activity.[8d]

Ruthenium is considered as an alternative to Pt in HOR/HER catalysts owing to the appropriate strength of Ru—H bonds and lower price.[13] A high surface area of the catalyst support is of great significance for the heterogeneous catalyst since it creates a high metal–support interface. Transition metal carbides (TMCs) have evoked special attention because of their Pt-like catalytic properties, good electrical conductivity, and strong oxidation resistance.[14] In various precious metal catalysts, tungsten carbide has been recognized as an essential component or support, such as Pd_3Ni/WC, $Pt-WC_{1-x}$/MWNT, 5% Pt/WC, and others.[15] There have been many attempts to improve the electrocatalytic activity for HOR, methanol oxidation reaction (MOR), and oxygen reduction reaction (ORR) by using tungsten carbide.[16] Compared with carbon supports, the electrochemically active surface areas (ECSAs) of noble metal loaded on W_2C or WC has increased by 2–3 times owing to hydrogen spillover,[17] which refers to the migration of activated hydrogen atoms from the noble metal particles to the catalyst support surface.[18] In addition, metals and metal oxides are typical supports due to their interfacial synergies and strong metal–support interaction.[19] For instance, WO_3 was also used as a carrier for noble metal particles due to hydrogen spillover,[18] enhancing the interaction between active components and supports. The W ions can act as Lewis acid sites to adsorb H_2O molecules on WO_3 surface, but the interaction between adsorbed H_2O and W is not strong enough to hold H_2O on the surface, as demonstrated by detailed density functional theory (DFT) calculations, which may benefit water dissociation.[20]

Accordingly, we reported a bifunctional $Ru/NC@WO_3-W_2C$ (Ru/NC@WOC) catalyst that can be used for HOR and HER electrocatalysis. In other words, we attempt to design a system that couples HOR with HER to realize the mutual conversion of electricity and hydrogen energy. A series of different loadings of Ru clusters with an average size of approximately 1.79 nm based

0.26 nm, consistent with distances of W_2C (101) and (100) planes. Furthermore, the high-angle annular dark-field scanning transmission electron microscopy (HAADF-STEM) image and energy-dispersive X-ray spectroscopy (EDS) element mapping images are shown in Figure 1d. It revealed that C, N, O, W, and Ru elements are distributed uniformly in Ru/NC@WOC nanostructures. The morphological features produce Brunauer-Emmett-Teller (BET) surface areas of 324.07 m^{2}g^{-1} for Ru/NC@WOC. The pore-size distribution examined by the Barrett-Joyner-Halenda (BJH) method was 6.4 nm, proving that Ru/NC@WOC is a typical mesoporous material (Figure 1c).[25] There are two predominant Raman peaks at around 1360 and 1560 cm^{-1} representing D- and G-bands (Figure S3).[26] The D-band is ascribed to the vibration of disordered and defective graphite, while the G-band is related to graphitic lattice phonon.[27] With the increase of calcination temperature, the graphitization degree of carbon materials is improved. Compared with Ru/NC@W$_2$C-800 C and Ru/NC@W$_2$C-900 C, Ru/NC@WOC has a smaller I_D/I_G value, which is probably due to the synergy of defective carbon and graphitized carbon atoms contributing to the formation of highly conductive materials at the appropriate temperature.[25,28] The I_D/I_G value of around 0.83 can be observed for the different loading of Ru species, indicating the same degree of graphitization.

X-ra oo l c ro c ro co

The valence states and compositions of the sample were obtained by X-ray photoelectron spectroscopy (XPS). The full survey spectrum of Ru/NC@WOC containing C, N, O, W, and Ru is shown in Figure 2a, which is well-aligned with the XRD and TEM results. Eight binding energy (BE) peaks can be deconvoluted in the C 1 s + Ru 3d XPS spectrum of Ru/NC@WOC (Figure 2b). The peaks at BEs of 284.0, 284.8, 286.0, and 287.7 eV were readily attributed to C=C, C–C/C–N, C–O, and C=O, whereas Ru 3d peaks are observed at BEs of 288.0 (Ru^0 3d$_{5/2}$), 283.8 (Ru^0 3d$_{3/2}$), 281.1 (RuO$_2$ 3d$_{5/2}$), and 285.2 eV (RuO$_2$ 3d$_{3/2}$).[29] Two couplets of peaks were observed in the Ru 3p spectrum (Figure 2c). The peaks centered at 461.7 and 483.8 eV are ascribed to Ru 3p$_{3/2}$ and Ru 3p$_{1/2}$. The two smaller peaks at BEs of 464.8 and 486.7 eV attributable to the RuO$_2$ 3p$_{3/2}$ and RuO$_2$ 3p$_{1/2}$, which possibly originated from air exposure during XPS analysis.[13b] Four peaks at 31.4, 33.1, 34.7, and 36.9 eV were assigned to W 4f. The relatively weak bands at 31.4 and 33.1 eV were indexed to W–C bonding, while the other two can be assigned to W–O binding energies (Figure 2d).[30] As presented in Figure 2e, the N 1 s XPS spectrum shows four peaks of N species at 396.8, 398.8, 399.9, and 401.1 eV, namely W–N, pyridinic-N, pyrrolic-N, and graphitic-N species.[31] The O 1 s XPS spectrum (Figure 2f) was fitted by three deconvoluted peaks at 530.2 (M–O), 531.8 (C=O), and 532.7 eV (H$_2$O$_{ads}$), further demonstrating the existence of WO$_3$-W$_2$C.[32]

l c roc c t o k R

The pyrolysis temperature is of paramount importance for the catalytic activity of HOR.[33] It is thus essential to optimize the calcination temperature. The HOR polarization curves (Figure 3a) showed that Ru/NC@WOC calcined at 700 C shows the best performance. The cyclic voltammograms (CVs) of these catalysts are displayed in Figure S4. Note that the electrochemical data reported here was the uncompensated ohmic drop with *iR* correction (Figure S5). Electrochemical impedance spectroscopic (EIS) results revealed that Ru/NC@WOC has relatively lower resistances than Ru/C and therefore a faster charge transfer.[34]
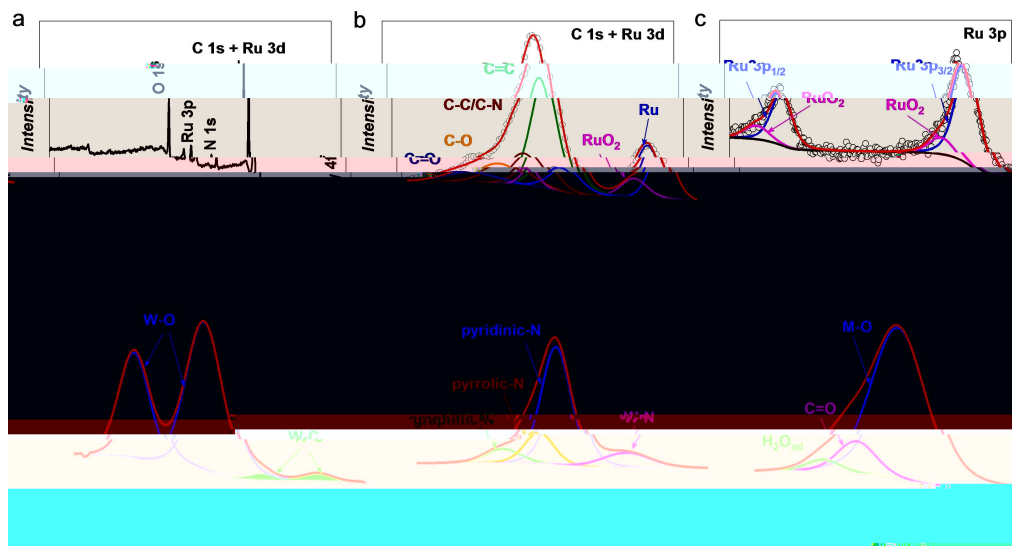
ChemSusChem

Full Papers
doi.org/10.1002/cssc.202100893

**Chemistry
Europe**
European Chemical
Societies Publishing

Figure 2. (a) XPS survey spectrum of Ru/NC@WOC. (b–f) High-resolution XPS spectra of C 1s + Ru 3d, Ru 3p, W 4f, N 1s, and O 1s for Ru/NC@WOC.
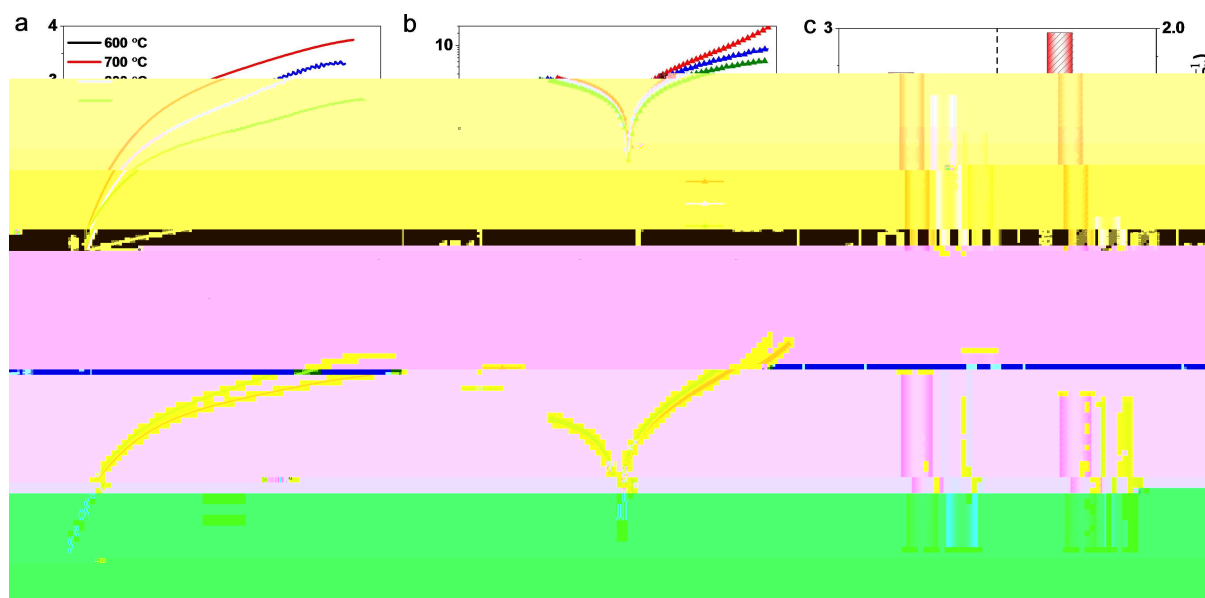

Figure 3. (a) HOR polarization curves of Ru/NC@WO₃-600 °C, Ru/NC@WOC, Ru/NC@W₂C- 800 °C, and Ru/NC@W₂C-900 °C in H₂-saturated 0.1 M KOH with a rotation rate of 1600 rpm at 10 mV s⁻¹. (b) HOR/HER Tafel plots of kinetic current density (j_k). (c) Comparison of the exchange current density (j_0) and mass activities $j_{k,m}$ at 50 mV of different studied catalysts. (d) HOR polarization curves of Ru/NC@WOC at different loadings of Ru species. (e) HOR/HER Tafel plots of j_k. (f) Comparison of the j_0 and $j_{k,m}$ at 50 mV of different studied catalysts.

current density (j_k) versus the overpotential (Figure 3b). The exchange-current density (j_0) was obtained from the micro-polarization region (−5 to 5 mV) by linear fitting through the Butler-Volmer equation.[35] The slope is directly proportional to j_0 (Figure S6). As displayed in Figure 3c, the Ru/NC@WOC shows a j_0 of 2.4 mA cm⁻², which is higher than Ru/NC@WO₃-600 °C (0.23 mA cm⁻²), Ru/NC@W₂C-800 °C (2.1 mA cm⁻²), and Ru/NC@W₂C-900 °C (1.6 mA cm⁻²). We also calculated the j_k normalized with the precious metal loading at 0.05 V (vs. RHE) (Figure 3c). It appears that the sequence of mass activity is: Ru/NC@WOC (1.96 mA μg_{Ru}^{-1}) > Ru/NC@W₂C-800 °C (0.31 mA μg_{Ru}^{-1})

> Ru/NC@W₂C-900 °C (0.16 mA μg_{Ru}^{-1}) > Ru/NC@WO₃-600 °C (0.0093 mA μg_{Ru}^{-1}), further verifying the pyrolysis temperature of the support is a crucial factor for HOR catalysis. Meanwhile, the Ru loading was also optimized. As shown in Figure 3d, we found that a higher Ru loading indicated a higher HOR current density, in which the exchange current density of Ru/NC@WOC (2.4 mA cm⁻²) increases 1.5 times compared to that of Ru₄.₄/NC@WOC (1.6 mA cm⁻²). Still, the increment is only 1.13 times when the Ru content increases from 6.3 to 9.1 wt% (2.7 mA cm⁻²). Figure 3e shows the Tafel plots of these three samples. Simultaneously, the mass activity is calculated to be

These are not the final page numbers! ↗↗

ChemSusChem

Full Papers
doi.org/10.1002/cssc.202100893

Chemistry
Europe
European Chemical
Societies Publishing

1.84, 1.96, and 0.21 mA μg_{Ru}^{-1} for $Ru_{9.1}$/NC@WOC, Ru/NC@WOC, and $Ru_{4.4}$/NC@WOC (Figure 3f).

It is generally accepted that HBE is closely related to HOR/HER activity.[8b] The complete desorption potential of H on the electrocatalyst representing the H binding strength and faster HOR kinetics is benefited from the sites with weaker HBE in alkaline media.[36] Next, we studied the electrocatalytic HOR performance of Ru/NC@WOC, NC@WOC, commercial Pt/C catalysts, and benchmark Ru/C. CVs of these three catalysts in N_2-saturated 0.1 M KOH electrolyte are indicated in Figure 4a. Ru/NC@WOC and commercial Pt/C exhibited the typical characteristic peaks of hydrogen adsorption/desorption in 0 and 0.4 V (vs. RHE) range. The $E_{H\text{-}desorption}$ negatively shifts from commercial Pt/C (0.311 V vs. RHE) to Ru/NC@WOC (0.227 V vs. RHE), indicating reduced HBE.[36,37] However, the NC@WOC and benchmark Ru/C showed unremarkable hydrogen adsorption/desorption peak, demonstrating the importance of interaction between metal and supports.[38] Thus, we can conclude that Ru/NC@WOC with weaker HBE possesses higher HOR kinetics superior to commercial Pt/C. The HOR polarization curves (Figure 4b) displayed that the anode current density of Ru/NC@WOC is higher than commercial Pt/C and benchmark Ru/C across the whole potential range. Ru/NC@WOC performed a better HOR activity than Ru/C at the same Ru loading, substantiating the significance of well-dispersed Ru clusters supported on the NC@WOC matrix in promoting hydrogen oxidation. The j_0 is evaluated from the micro-polarization linear region (−5 to 5 mV), and Ru/NC@WOC shows higher slope than Pt/C and Ru/C, suggesting the higher HOR activity (Figure S6c). Simultaneously, the NC@WOC has negligible impact on HOR activity; therefore, the Ru was considered the active component of Ru/NC@WOC. Figure S7 showed Ru/NC@WOC's polarization curves in N_2-saturated 0.1 M KOH; only a small anode current was observed, indicating the H_2 is a reactant for HOR. We investigated Ru/NC@WOC's polarization curves as a function of rotating speeds (Figure S8). The current density grows with the increase of rotational rate due to mass transport promotion at higher rotating speed.[35] The inset of polarization curves showed the Koutecky-Levich plot of Ru/NC@WOC at an overpotential of 25 mV, which showed that the inverse of j is in direct proportion to $\omega^{1/2}$ (the square root of rotation rate). The HOR/HER Tafel plots of j_k on Ru/NC@WOC, NC@WOC, commercial Pt/C, and benchmark Ru/C are shown in Figure 4c. The accelerated durability tests (ADTs) were conducted in 0.1 M KOH under continuous N_2 flow by cycling the potential from 0 to 1.0 V (vs. RHE) at 100 mV s^{-1} for 1000 cycles. Alkaline HOR polarization curves of Ru/NC@WOC before and after 1000 CV cycles are displayed in Figure 4d. The polarization curves almost overlap, demonstrating the favorable stability of Ru/NC@WOC. Besides, the durability of Ru/NC@WOC and commercial Pt/C was assessed by chronoamperometry at low potential $\eta =$ 0.05 V (vs. RHE) and high potential $\eta = 0.15$ V (vs. RHE) in H_2-satuared 0.1 M KOH while rotating them at 1600 rpm (Figure S9). Ru/NC@WOC maintained a stable current density of approximately 2.6 and 3.7 mA cm^{-2} throughout the test, which contrasted with the gradual activity loss of commercial Pt/C. At 0.05 V (vs. RHE), j_k of 63.07 mA cm^{-2} was obtained for Ru/NC@WOC, which is 4.7 times as high as that of Pt/C benchmark. Moreover, it exhibited up 30-fold HOR improvement in j_k compared with benchmark Ru/C. The Ru/NC@WOC shows j_0 of 2.4 mA cm^{-2}, which exceeds that of 2.0 and 1.0 mA cm^{-2} for commercial Pt/C and benchmark Ru/C (Figure 4e). As illustrated in Figure 4f and Table S3, Ru/NC@WOC shows much better HOR performance compared with Pt/C benchmark and other
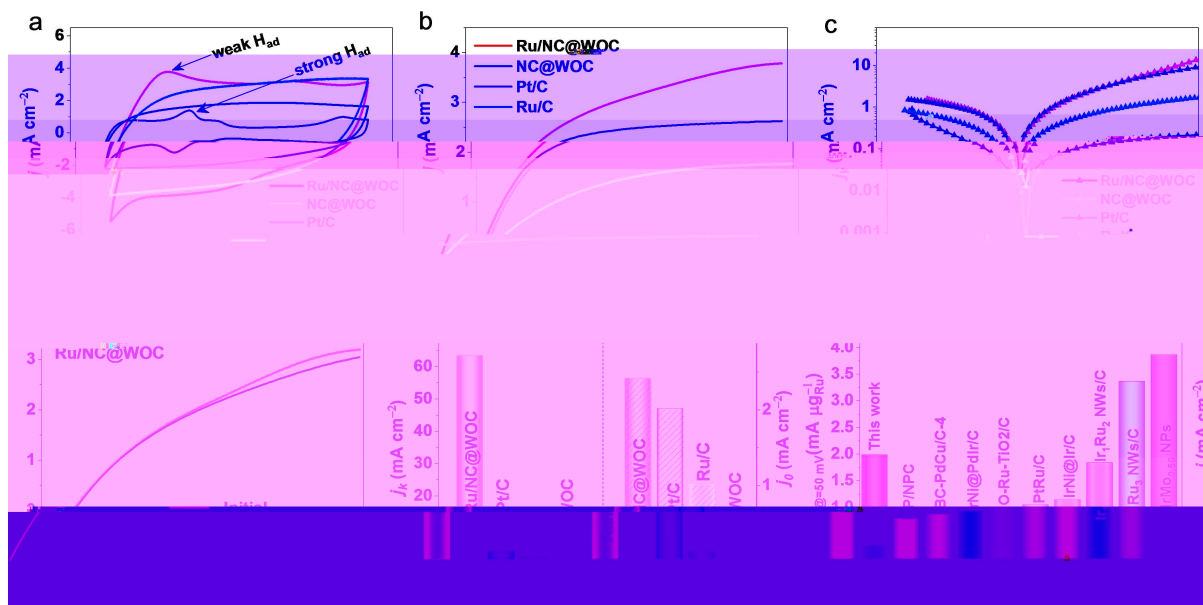

Figure 4. (a) CVs of Ru/NC@WOC, NC@WOC, commercial Pt/C, and benchmark Ru/C in N_2-saturated 0.1 M KOH. (b) HOR polarization curves of Ru/NC@WOC, NC@WOC, commercial Pt/C, and benchmark Ru/C in H_2-saturated 0.1 M KOH; rotating speed: 1600 rpm, scan rate: 10 mV s^{-1}. (c) Representative HOR/HER Tafel plots of j_k for Ru/NC@WOC, NC@WOC, commercial Pt/C, and benchmark Ru/C. (d) Accelerated durability test results of Ru/NC@WOC. (e) j_k at 50 mV and j_0 of different studied catalysts. (f) $j_{k,m}$ at 50 mV of Ru/NC@WOC and alkaline HOR electrocatalysts in the literature.

reported HOR electrocatalysts. Moreover, we summarized the metal loading, ECSA, $j_{k,m}$ at 50 mV, SA at 50 mV, j_k at 50 mV, and j_0 in Table 1. As Ru would block the sites for desorption and adsorption of hydrogen, it is not suitable to use hydrogen underpotential deposition (H-UPD) region to calculate the ECSAs.[39] The ECSAs of samples were measured via CO stripping voltammetry. As presented in Figure 5a–c and Figure S10, the ECSA of Ru/NC@WOC was calculated to be 161.5 m² g⁻¹, which is 3.3 times higher than the Pt/C benchmark (48.1 m² g⁻¹) and 10 times higher than the Ru/C benchmark (15.8 m² g⁻¹). The ECSAs of other catalysts were summarized in Table 1.

Electrocatalytic of Alkaline HER

HER is the reverse reaction of HOR. The HER tests were performed in H₂-saturated 1.0 M KOH electrolyte. During the measurement, high-purity H₂ is bubbled through the electrolyte to saturated it, fix the reversible hydrogen potential, and prevent the dissolution and absorption of CO₂.[40] Initially, the HER performance of the as-prepared catalysts was optimized by varying the annealing temperature of support from 600 to 900 C at the same metal loading. The results indicated that catalyst activity with support at an annealing temperature of 700 C was highest, along with the smallest Tafel slope (Figure S11). Similarly, we also explore the effect of Ru loading on catalytic performances. Linear sweep voltammetry (LSV) curves manifested that the catalyst with a Ru loading of 6.3 wt% shows the lowest potential at 10 mA cm⁻² (Figure S11). Meanwhile, we performed a comparative study of the HER activities of Ru/NC@WOC, NC@WOC, commercial Pt/C, and Ru/C benchmark.

Figure 6a shows the polarization curves of these four catalysts. The Ru/NC@WOC displayed a similar HER performance with lower overpotential of 31 mV to yield 10 mA cm⁻² compared with commercial Pt/C (32 mV) and benchmark Ru/C (64 mV). The NC@WOC is inert for HER catalysis. Moreover, we summarized the corresponding overpotential at different current densities (Figure 6e). Over potentials of Ru/NC@WOC at various current densities (31 mV at 10 mA cm⁻², 88 mV at 50 mA cm⁻², and 119 mV at 100 mA cm⁻²) are significantly lower than those of the commercial Pt/C (32 mV at 10 mA cm⁻², 111 mV at 50 mA cm⁻², and 194 mV at 100 mA cm⁻²) and the Ru/C benchmark (64 mV at 10 mA cm⁻², 147 mV at 50 mA cm⁻², and 206 mV at 100 mA cm⁻²). The corresponding Tafel slopes are 40.5, 40.7, 63.2, and 186.6 mV dec⁻¹ for Ru/NC@WOC, commercial Pt/C, benchmark Ru/C, and NC@WOC (Figure 6b). It is shown that the highly efficient HER kinetics on the Ru/NC@WOC follows the Volmer–Heyrovsky mechanism associated with the electrochemical desorption of hydrogen, which is the rate-limiting step.[34] The solution resistance reflects the impedance between the working electrode and the reference electrode circuit, which is mainly affected by changes in the experimental setup (Figure S12), while the charge transfer resistance mainly explores the conductivity of the catalyst. As illustrated in Figure 6c, Ru/NC@WOC shows a much smaller semicircle than that of commercial Pt/C and the Ru/C benchmark in complex-plane plot, demonstrating Ru/NC@WOC has a smaller charge transfer resistance with higher conductivity during the HER catalysis.[41] The stability of Ru/NC@WOC was observed with LSV after cycling 1000 CVs at a sweep rate of 100 mV s⁻¹ between 0–1.0 V (vs. RHE) (Figure S13). Then, the overpotential of Ru/NC@WOC at 10 mA cm⁻² increased by

Table 1. Summary of ECSA, $j_{k,m}$, SA, j_k, and j_0 of different catalysts in this work.[a]

Catalyst	ECSA [m² g⁻¹]	$j_{k,m}$ [mA μg⁻¹]	SA [mA cm⁻²]	j_k [mA cm⁻²]	j_0 [mA cm⁻²]
Pt/C	48.1	0.26	0.55	13.35	2.0
Ru/C	15.8	0.07	0.43	2.17	1.0
Ru₄.₄/NC@WOC	69.4	0.21	0.30	4.73	1.6
Ru/NC@WOC	161.5	0.75	0.47	77.7	2.9
Ru₉.₁/NC@WOC	138.4	1.84	1.33	85.51	2.7
Ru/NC@WO₃(600)	2.6	0.0093	0.006	0.298	0.23
Ru/NC@W₂C(800)	141.6	0.31	0.20	9.81	2.1
Ru/NC@W₂C(900)	112.2	0.16	0.13	5.01	1.6

[a] $j_{k,m}$: mass activity at 50 mV. SA: specific activity. j_k: kinetic current density at 50 mV. j_0: exchange current density from the micro-polarization region (−5 to 5 mV) by linear fitting through the Butler-Volmer equation.
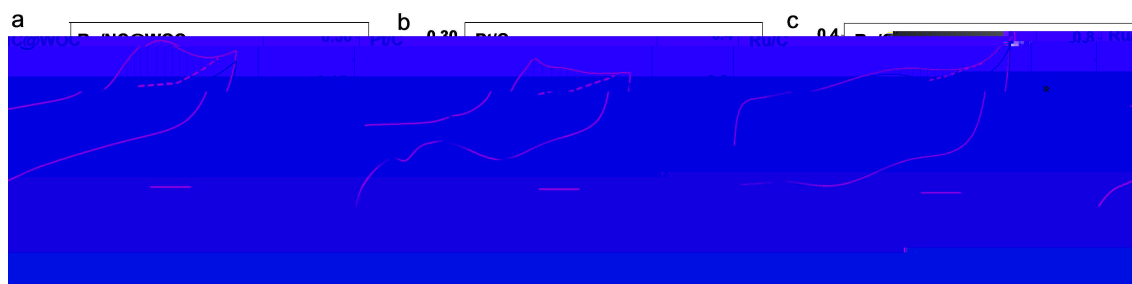

Figure 5. CO-stripping voltammetry of (a) Ru/NC@WOC, (b) Pt/C, and (c) benchmark Ru/C in 0.1 M KOH solution.

These are not the final page numbers! ↗↗

13 mV after 1000 cycles, suggesting good stability of Ru/NC@WOC. Additionally, we also evaluated the durability of Ru/NC@WOC and the commercial Pt/C by chronopotentiometry. A negligible decline was observed from Ru/NC@WOC during the test, indicating comparable durability to that of commercial Pt/C catalysts (Figure S14). The turnover frequency (TOF) value was calculated using ICP results (see Table S1) to assess per-site instinct activity quantitatively.[42] The TOF values of commercial Pt/C and the Ru/C benchmark are only 0.014 and 0.012 s^{-1} at an overpotential of 100 mV. In comparison, the TOF of Ru/NC@WOC is 0.033 s^{-1}, obviously demonstrating the HER catalytic performance of Ru/NC@WOC surpasses that of the Pt/C benchmark and the Ru/C benchmark (Figure 6d). Furthermore, the HER activity of Ru/NC@WOC exhibits much lower overpotential than that of Ru-based electrocatalysts reported in recent years (Figure 6f and Table S4).

Catalytic mechanism of HER/HOR

The combination of metal Ru and n-type WO$_3$ semiconductor could generate a heterogeneous interface. Since the work function of Ru metal (4.7 eV) is smaller than the Fermi level of n-type WO$_3$ semiconductor (5.05 eV), part of electrons would be transferred from metallic Ru to WO$_3$ to form electron-deficient Ru and electron-rich n-type WO$_3$.[43] DFT calculations by Jiang et al. have shown that the Gibbs free energy of hydrogen adsorption (G_{H^*}) (−0.44 eV) of Ru$_2$P/WO$_3$@NPC is closer to 0 than that of WO$_3$@NPC (−0.82 eV), indicating the Ru sites can be favorable for the adsorption and desorption of hydrogen.[22] Albanese et al. have demonstrated that W sites on WO$_3$ facilitate the adsorption of H$_2$O, and the interaction of H$_2$O$_{ads}$ and W is not very strong, which is beneficial to H$_2$O$_{ads}$ dissociation.[20] For

the HER mechanism, we can conclude the positively charged Ru sites and negatively charged WO$_3$ facilitate dissociative of H$_2$O$_{ads}$ from WO$_3$ and accelerate the adsorption and desorption of hydrogen from Ru sites to form H$_2$ in alkaline media. Besides, the role of W$_2$C is not negligible, providing high electrical conductivity. As the OH adsorption on the metal surface is widely accepted as the rate-determining step of HOR activity in alkaline medium, we performed CO stripping experiments to investigate OH adsorption on the Ru sites.[7c] CO stripping voltammetry curves of Ru/NC@WOC and Ru/NC@W$_2$C-900 °C are displayed in Figure 5 and Figure S9; Ru/NC@WOC shows a CO stripping peak potential of 0.80 V. In contrast, Ru/NC@W$_2$C-900 °C shows a peak at 0.74 V, revealing WO$_3$ mainly regulated the adsorption of OH. That is, WO$_3$ provides OH adsorption sites, and Ru serves as active site for H adsorption. H$_{ads}$ desorption on Ru sites increases the reactivity of OH$_{ads}$ desorption to form H$_2$O.

Based on the above results, the encouraging HOR/HER performance in alkaline electrolyte could arise from the following aspects: 1) strong electronic interaction between Ru and NC@WOC substrate; 2) Ru

Conclusion

A cost-effective bifunctional catalyst of Ru/NC@WO$_3$–W$_2$C is fabricated via co-precipitation and polyol reduction methods. The calcination temperature of the support plays a fundamental role in the electrocatalytic activity of hydrogen oxidation/evolution reactions (HOR/HER). During annealing from 600 to 900 °C, a phase transformation was observed between WO$_3$ and W$_2$C. The Ru/NC@WOC sample, featuring WO$_3$ phase and W$_2$C phase, exhibits higher mass activity and exchange-current density of HOR than commercial Pt/C in alkaline media. Moreover, Ru/NC@WOC shows an outstanding electrocatalytic H$_2$ production capacity with overpotentials of 31 and 119 mV at 10 and 100 mA cm^{-2} in alkaline media. The high HOR/HER activities can be ascribed to the synergy between the three components Ru, WO$_3$, and W$_2$C. Systematic investigations further demonstrated that WO$_3$ offers OH adsorption sites and Ru provides adsorption sites for H, endowing Ru/NC@WOC with outstanding HOR activity. For the enhancement of HER activity, the electron donation from Ru to W promotes the dissociation of H$_2$O and desorption of H$_{ads}$, releasing H$_2$ gas. Our work provides a rational strategy for developing a low-cost and stable bifunctional electrocatalyst as an alternative to Pt/C for fuel cells and water electrolyzers.

Supporting Information

Details on materials, synthesis procedures, characterizations, electrochemical measurements, impedance spectroscopy study, and HOR and HER comparison tables are given in the Supporting Information.

Conflict of

ChemSusChem

Full Papers
doi.org/10.1002/cssc.202100893

Chemistry
Europe
European Chemical
Societies Publishing

[28] H. Ren, Y. Wang, Y. Yang, X. Tang, Y. Peng, H. Peng, L. Xiao, J. Lu, H. D. Abruña, L. Zhuang, *ACS Catal.* **2**, 7, 6485–6492.

[29] J. Guo, C. Wu, J. Zhang, P. Yan, J. Tian, X. Shen, T. T. Isimjan, X. Yang, *J. Mater. Chem. A* **2**, 7, 8865–8872.

[30] J. Chen, B. Ren, H. Cui, C. Wang, *Small* **2 2**, 16, e1907556.

[31] B. Xiong, W. Zhao, L. Chen, J. Shi, *Adv. Funct. Mater.* **2**, 29, 1902505.

[32] G. Meng, H. Tian, L. Peng, Z. Ma, Y. Chen, C. Chen, Z. Chang, X. Cui, J. Shi, *Nano Energy* **2 2**, 80, 105531.

[33] H. Peng, Z. Mo, S. Liao, H. Liang, L. Yang, F. Luo, H. Song, Y. Zhong, B. Zhang, *Sci. Rep.* **2**, 3, 1765.

[34] Y. Hu, H. Yu, L. Qi, J. Dong, P. Yan, T. T. Isimjan, X. Yang, *ChemSusChem* **2 2**, 14, 1565–1573.

[35] Y. Duan, Z.-Y. Yu, L. Yang, L.-R. Zheng, C.-T. Zhang, X.-T. Yang, F.-Y. Gao, X.-L. Zhang, X. Yu, R. Liu, H.-H. Ding, C. Gu, X.-S. Zheng, L. Shi, J. Jiang, J.-F. Zhu, M.-R. Gao, S.-H. Yu, *Nat. Commun.* **2 2**, 11, 4789.

[36] B. Qin, H. Yu, X. Gao, D. Yao, X. Sun, W. Song, B. Yi, Z. Shao, *J. Mater. Chem. A* **2**, 6, 20374–20382.

[37] Y. Cong, I. T. McCrum, X. Gao, Y. Lv, S. Miao, Z. Shao, B. Yi, H. Yu, M. J. Janik, Y. Song, *J. Mater. Chem. A* **2**, 7, 3161–3169.

[38] M. Ming, Y. Zhang, C. He, L. Zhao, S. Niu, G. Fan, J.-S. Hu, *Small* **2**, 15, 1903057.

[39] N. Danilovic, R. Subbaraman, D. Strmcnik, A. P. Paulikas, D. Myers, V. R. Stamenkovic, N. M. Markovic, *Electrocatalysis* **2 2**, 3, 221–229.

[40] a) J. Mao, C.-T. He, J. Pei, W. Chen, D. He, Y. He, Z. Zhuang, C. Chen, Q. Peng, D. Wang, Y. Li, *Nat. Commun.* **2**, 9, 4958; b) S. Xue, R. W. Haid, R. M. Kluge, X. Ding, B. Garlyyev, J. Fichtner, S. Watzele, S. Hou, A. S. Bandarenka, *Angew. Chem. Int. Ed.* **2 2**, 59, 10934–10938; *Angew. Chem.* **2 2**, 132, 11026–11031.

[41] J. Yang, G. Ning, L. Yu, Y. Wang, C. Luan, A. Fan, X. Zhang, Y. Liu, Y. Dong, X. Dai, *J. Mater. Chem. A* **2**, 7, 17790–17796.

[42] B. Wang, H. Huang, T. Sun, P. Yan, T. T. Isimjan, J. Tian, X. Yang, *J. Colloid Interface Sci.* **2 2**, 567, 339–346.

[43] a) G. Halek, I. D. Baikie, H. Teterycz, P. Halek, P. Suchorska-Woźniak, K. Wiśniewski, *Sens. Actuators B* **2**, 187, 379–385; b) L. Li, Y. Wang, S. Vanka, X. Mu, Z. Mi, C.-J. Li, *Angew. Chem. Int. Ed.* **2**, 56, 8701–8705; *Angew. Chem.* **2**, 129, 8827–8831.

These are not the final page numbers! ↗↗

FULL A R S

T o b r o o : A cost-effective bifunctional catalyst, Ru/NC@WO$_3$-W$_2$C, is fabricated by co-precipitation and polyol reduction. Electrochemical studies find that the designed catalyst has excellent hydrogen oxidation/evolution (HOR/HER) catalytic activity and stability in alkaline electrolyte.

Efficient Bifunctional

Ru/NC@WOC

Y. Yang, X. Shao, S. Zhou, P. Yan, Dr. T. T. Isimjan*, Prof. Dr. X. Yang*

1 – 10

r l c ro c C l o
C$_5$W -W$_2$C cor R
C r R r bl C
o l c roc c ro
o ol o R o